ADAPTIVE SOLUTION OF PHASE CHANGE PROBLEMS OVER UNSTRUCTURED TETRAHEDRAL MESHES

R.H. NOCHETTO*, A. SCHMIDT† AND C. VERDI‡

Abstract. We discuss the two main ingredients for the adaptive numerical solution of phase change problems, that is a posteriori error estimation and mesh modification in 2d and 3d via refinement and coarsening for unstructured tetrahedral meshes. We illustrate our adaptive algorithm with a number of numerical experiments.

1. Introduction. The essential ingredients for a reliable and efficient adaptive method to approximate (nonlinear) evolution PDEs are:

(a) computable *a posteriori error estimators* that measure both the space and time discretization errors in suitable norms with information extracted from the discrete solution and data;

(b) an efficient *mesh generator* that performs refinement and coarsening of an (unstructured) grid with local information provided by the a posteriori error estimators.

A posteriori error estimators must be taylored to the problem at hand by evaluating the residual in suitable negative norms, and thereby properly capturing its oscillatory and singular behavior. The mesh generator is, instead, a general purpose tool with the same basic principles irrespective of the problem. In this paper, we review both issues in the context of phase changes [12], [13], [14].

Phase change problems exhibit regions of relatively smooth behavior (phases) separated by free boundaries (interfaces) across which regularity lacks. This in turn results in global numerical pollution effects. A cure consists of equidistributing discretization errors in adequate norms by means of highly graded meshes and varying time steps. Their design, rigorous analysis, and efficient implementation constitute the main thrust of this paper.

We consider for simplicity the classical two-phase Stefan problem

$$\partial_t u - \Delta\beta(u) = f \quad \text{in } Q = \Omega \times (0,T), \tag{1.1}$$

with $u(\cdot,0) = u_0(\cdot)$ in Ω and $\beta(s) = \min(s,0) + \max(s-1,0)$; this corresponds to an ideal material with constant thermal properties and unit latent heat. A discrete solution U of (1.1) satisfies $U(\cdot,0) = U^0(\cdot)$ and

$$\partial_t U - \Delta\beta(U) = f - \mathcal{R} \quad \text{in } Q, \tag{1.2}$$

* Department of Mathematics, University of Maryland, College Park, MD 20742, USA. Partially supported by NSF Grant DMS-9623394 and NSF SCREMS 9628467.

† Institut für Angewandte Mathematik, Universität Freiburg, 79104 Freiburg, Germany. Partially supported by EU Grant HCM "Phase Transitions and Surface Tension".

‡ Dipartimento di Matematica, Università di Milano, 20133 Milano, Italy. Partially supported by MURST and CNR Contract 95.00735.01.

where $\mathcal{R}$, a distribution with singular components and oscillatory behavior, is the so-called *parabolic residual.* We will show below that evaluating $\mathcal{R}$ for the degenerate parabolic problem (1.1) is intrinsically distinct from previous work done for the heat equation [3] or mildly nonlinear variants of it [4]. The presence of free boundaries and limited regularity will play a crucial role.

The error $e_u = u - U$ can be represented in terms of $\mathcal{R}$, which leads to an error estimate of the form

$$\|e_u(\cdot,T)\|_{H^{-1}(\Omega)} \le \mathcal{E}(U,f,T,\Omega;h,\tau),$$

with computable right hand side; hereafter h stands for the meshsize and τ for the time step. This formula is derived in §§2-4, and forms the basis of the adaptive algorithm of §5. The resulting quasi-optimal meshes are further examined in §6. Implementation issues such as refinement and coarsening operations using bisection in 2d and 3d, along with accompanying hierarchical data structures, are discussed in §7. We conclude in §8 with several illuminating simulations that clearly demonstrate the computational gains obtained via adaptivity.

2. Error Representation. Upon subtracting (1.2) from (1.1), the error e_u satisfies the equation

$$\partial_t e_u - \Delta(b e_u) = \mathcal{R} \tag{2.1}$$

in the sense of distributions, where

$$0 \le b(x,t) = \int_0^1 \beta'(su(x,t) + (1-s)U(x,t))\,ds \le 1$$

is discontinuous. To express e_u in suitable norms we resort to *parabolic duality.* We multiply (2.1) by a smooth test function ϕ and integrate by parts, thereby obtaining

$$\langle e_u(\cdot,T), \phi(\cdot,T)\rangle = \langle u_0 - U^0, \phi(\cdot,0)\rangle + \int_0^T \langle e_u, \partial_t\phi + b\Delta\phi\rangle + \mathcal{R}(\phi), \tag{2.2}$$

where $\langle\cdot,\cdot\rangle$ stands for the inner product in $L^2(\Omega)$. We are thus led to study the backward parabolic problem in *nondivergence* form [9], with vanishing diffusion coefficient b and regularization parameter $\delta \downarrow 0$,

$$\partial_t\phi + (b+\delta)\Delta\phi = 0 \quad \text{in } Q, \qquad \phi(\cdot,T) = \rho \quad \text{in } \Omega. \tag{2.3}$$

The theory of nonlinear strictly parabolic problems [6] yields existence of a unique solution ψ, which satisfies the stability bounds [12]

$$\max_{0\le t\le T} \|\nabla\phi(\cdot,t)\|_{L^2(\Omega)},\ \|\partial_t\phi\|_{L^2(Q)},\ \delta^{1/2}\|\Delta\phi\|_{L^2(Q)} \le \|\rho\|_{H_0^1(\Omega)}. \tag{2.4}$$

For the heat equation $b = 1$, instead, we have [3] for all $0 \le t \le T$

$$\|\phi(\cdot,t)\|_{L^2(\Omega)},\ (T-t)\|\partial_t\phi(\cdot,t)\|_{L^2(\Omega)} \le \|\rho\|_{L^2(\Omega)}. \tag{2.5}$$

We thus realize that (2.3) does not exhibit a regularizing effect such as (2.5) since $\phi(\cdot,t) = \rho$ for $b = \delta = 0$; hence $\|\Delta\phi\|_{L^2(Q)}$ is never bounded uniformly in δ. We also see from (2.4) that the correct space for ρ is $H_0^1(\Omega)$ and not $L^2(\Omega)$. Duality combined with (2.2) thus yields

$$\|e_u(\cdot,T)\|_{H^{-1}(\Omega)} \le \|u_0 - U^0\|_{H^{-1}(\Omega)} + \sup_{\rho\in H_0^1(\Omega)} \frac{|\mathcal{R}(\phi)|}{\|\rho\|_{H_0^1(\Omega)}} + \delta^{1/2}A, \tag{2.6}$$

where $A = \|e_u\|_{L^2(Q)}$ is a priori bounded in terms of u_0 and f; in [12] we show how to circumvent this further assumption but we omit details here. We stress that U need not be a finite element approximation of u. We use (2.6) below to study the time and full discretizations of (1.1).

3. Time Discretization: A Posteriori Error Estimate. We first illustrate the main ideas for an implicit time discretization of (1.1).

Let $\tau_n = t^n - t^{n-1}$ be a variable time step and let U^n satisfy

$$\frac{U^n - U^{n-1}}{\tau_n} - \Delta\beta(U^n) = f^n, \tag{3.1}$$

where $f^n(\cdot)$ is an approximation of $f(\cdot,t)$ in $[t^{n-1},t^n]$; if $f^n(\cdot) = f(\cdot,t^n)$ then (3.1) is the backward Euler method. If $U(\cdot,t) = U^n$ for $t^{n-1} < t \le t^n$, then the residual $\mathcal{R}$ in (1.2) is given by

$$\mathcal{R} = \sum_{n=1}^N \Big(\frac{U^n - U^{n-1}}{\tau_n} + f - f^n\Big)\chi_{[t^{n-1},t^n]} - (U^n - U^{n-1})\delta_{t^{n-1}},$$

where χ_I is the characteristic function of I and δ_s is a Dirac mass at $t = s$. Equivalently, we can split $\mathcal{R}$ into $\mathcal{R}_1$ and $\mathcal{R}_2$ as follows

$$\mathcal{R}_1(\phi) = \sum_{n=1}^N \int_{t^{n-1}}^{t^n} \frac{1}{\tau_n}\langle U^n - U^{n-1}, \phi - \phi(\cdot,t^{n-1})\rangle, \tag{3.2}$$

$$\mathcal{R}_2(\phi) = \sum_{n=1}^N \int_{t^{n-1}}^{t^n} \langle f - f^n, \phi\rangle. \tag{3.3}$$

In view of (2.4) and $\phi(\cdot,t) - \phi(\cdot,t^{n-1}) = \displaystyle\int_{t^{n-1}}^t \partial_s\phi(\cdot,s)\,ds$, we deduce

$$\begin{aligned}|\mathcal{R}_1(\phi)| &\le \sum_{n=1}^N \int_{t^{n-1}}^{t^n} \|U^n - U^{n-1}\|_{L^2(\Omega)}\|\partial_t\phi\|_{L^2(\Omega)} \\ &\le \|\rho\|_{H_0^1(\Omega)}\Big(\sum_{n=1}^N \tau_n\|U^n - U^{n-1}\|^2_{L^2(\Omega)}\Big)^{1/2}.\end{aligned}$$

Similarly, if $f^n(\cdot) = \frac{1}{\tau_n}\int_{t^{n-1}}^{t^n} f(\cdot,s)\,ds = \bar{f}^n(\cdot)$, we can exploit L^2_t orthogonality to express and bound $\mathcal{R}_2$ as follows

$$
\begin{aligned}
|\mathcal{R}_2(\phi)| &= \Big|\sum_{n=1}^N \int_{t^{n-1}}^{t^n} \langle f - \bar{f}^n, \phi - \phi(\cdot, t^{n-1})\rangle\Big| \\
&\le \|\rho\|_{H^1_0(\Omega)} \Big(\sum_{n=1}^N \tau_n^2 \int_{t^{n-1}}^{t^n} \|f - \bar{f}^n\|^2_{L^2(\Omega)}\Big)^{1/2}.
\end{aligned}
$$

If we introduce the quantities

$$
\begin{aligned}
\mathcal{E}_0 &= \|u_0 - U^0\|_{H^{-1}(\Omega)} && \textit{initial error,} \\
\mathcal{E}_1 &= \Big(\sum_{n=1}^N \tau_n \|U^n - U^{n-1}\|^2_{L^2(\Omega)}\Big)^{1/2} && \textit{time residual,} \\
\mathcal{E}_2 &= \Big(\sum_{n=1}^N \tau_n^2 \int_{t^{n-1}}^{t^n} \|f - \bar{f}^n\|^2_{L^2(\Omega)}\Big)^{1/2} && \textit{interpolation,}
\end{aligned}
$$

we can take $\delta \downarrow 0$ in (2.6) to arrive at

$$
\|e_u(\cdot, T)\|_{H^{-1}(\Omega)} \le \mathcal{E}_0 + \mathcal{E}_1 + \mathcal{E}_2; \tag{3.4}
$$

the discretization error thus accumulates in time in the L^2 norm. Since

$$
\sum_{n=1}^N \|U^n - U^{n-1}\|^2_{L^2(\Omega)} \le C
$$

a priori in terms of $U_0 \in L^2(\Omega)$ and f, we realize that the above estimate is of *optimal* order $O(\max_n \tau_n^{1/2})$ under the weak regularity deal with. To make it computable, we can replace $\mathcal{E}_1$ by the upper bound

$$
\mathcal{E}_1 \le T^{1/2} \max_{1\le n\le N} \|U^n - U^{n-1}\|_{L^2(\Omega)}. \tag{3.5}
$$

Invoking H^1_x regularity of ϕ yields a weaker expression for $\mathcal{E}_2$ regardless of the choice of f^n [12]

$$
\mathcal{E}_2 = \sum_{n=1}^N \int_{t^{n-1}}^{t^n} \|f - f^n\|_{H^{-1}(\Omega)}.
$$

It is worth comparing (3.4) with the a posteriori error estimate for the heat equation [3]. In light of (2.5), $\mathcal{R}_1(\phi)$ in (3.2) can be bounded by

$$
\begin{aligned}
|\mathcal{R}_1(\phi)| &\le \sum_{n=1}^{N-1} \int_{t^{n-1}}^{t^n} \|U^n - U^{n-1}\|_{L^2(\Omega)} (T-t) \|\partial_t \phi\|_{L^2(\Omega)} (T-t)^{-1} \\
&\quad + \int_{t^{N-1}}^{t^N} \frac{1}{\tau_N} \|U^N - U^{N-1}\|_{L^2(\Omega)} \|\phi - \phi(\cdot, t^N)\|_{L^2(\Omega)} \\
&\le \log \frac{T}{\tau_N} \|\rho\|_{L^2(\Omega)} \max_{1\le n\le N} \|U^n - U^{n-1}\|_{L^2(\Omega)}.
\end{aligned} \tag{3.6}
$$

Likewise, if $f^n = \bar f^n$, then $\mathcal{R}_2$ in (3.3) becomes

$$\mathcal{R}_2(\phi) \le \log \frac{T}{\tau_N} \|\rho\|_{L^2(\Omega)} \max_{1\le n\le N} \int_{t^{n-1}}^{t^n} \|f - \bar f^n\|_{L^2(\Omega)}.$$

In view of (2.2) we infer the corresponding a posteriori error estimate

$$\begin{aligned} \|e_u(\cdot,T)\|_{L^2(\Omega)} \le \|u_0 - U^0\|_{L^2(\Omega)} & \qquad \textit{initial error} \\ + \log \frac{T}{\tau_N} \max_{1\le n\le N} \|U^n - U^{n-1}\|_{L^2(\Omega)} & \qquad \textit{time residual} \\ + \log \frac{T}{\tau_N} \max_{1\le n\le N} \int_{t^{n-1}}^{t^n} \|f - \bar f^n\|_{L^2(\Omega)} & \qquad \textit{interpolation.} \end{aligned}$$

We see that the error accumulation in time is quite different from (3.4) and (3.5), thereby reflecting the more stable behavior of the heat equation.

4. Full Discretization: A Posteriori Error Estimate. Let $\mathcal{M}^n$ be a uniformly regular partition of Ω into simplices, with meshsize density $h_n = h_S$ for $S \in \mathcal{M}^n$. Let $\mathbf{V}^n \subset H^1_0(\Omega)$ be the piecewise linear finite element space over $\mathcal{M}^n$ and I^n the Lagrange interpolation operator.

The discrete problem can be written as follows. Let $U^0 \in \mathbf{V}^0$ be an approximation of u_0. Given $U^{n-1}, \Theta^{n-1} \in \mathbf{V}^{n-1}$, then $\mathcal{M}^{n-1}$ and τ_{n-1} are modified as described in §5 to get $\mathcal{M}^n$ and τ_n and thereafter $U^n, \Theta^n \in \mathbf{V}^n$ computed according to $\Theta^n = I^n\beta(U^n)$ and

$$\frac{1}{\tau_n}\langle U^n - U^{n-1}, \varphi\rangle^n + \langle \nabla\Theta^n, \nabla\varphi\rangle = \langle f^n, \varphi\rangle^n \quad \forall\, \varphi \in \mathbf{V}^n, \tag{4.1}$$

where $\langle \varphi_1, \varphi_2\rangle^n = \int_\Omega I^n(\varphi_1\varphi_2)$ is the vertex rule. Mass lumping diagonalizes the mass matrix and, together with the constitutive relation $\Theta^n = I^n\beta(U^n)$ being only enforced at the nodes, leads to a monotone problem easy to implement and solved via an optimized nonlinear SOR [11].

On using (4.1) in (3.2) and (3.3), we easily arrive at

$$\begin{aligned} \mathcal{R}(\phi) = & \sum_{n=1}^N \int_{t^{n-1}}^{t^n} \langle R^n, \phi - \varphi\rangle \\ & - \sum_{n=1}^N \int_{t^{n-1}}^{t^n} \langle \nabla\Theta^n, \nabla(\phi - \varphi)\rangle \\ & + \sum_{n=1}^N \langle U^{n-1} - I^n U^{n-1}, \phi(\cdot, t^{n-1})\rangle \\ & + \sum_{n=1}^N \int_{t^{n-1}}^{t^n} \frac{1}{\tau_n}\langle U^n - I^n U^{n-1}, \phi - \phi(\cdot, t^{n-1})\rangle \\ & + \sum_{n=1}^N \int_{t^{n-1}}^{t^n} \langle \nabla I^n\beta(U^n) - \nabla\beta(U^n), \nabla\phi\rangle \\ & + \sum_{n=1}^N \int_{t^{n-1}}^{t^n} \Big(\langle R^n, \varphi\rangle - \langle R^n, \varphi\rangle^n\Big) + \sum_{n=1}^N \int_{t^{n-1}}^{t^n} \langle f - I^n f^n, \phi\rangle \end{aligned}$$

for all $\varphi(\cdot,t) \in \mathbf{V}^n$, $t^{n-1} < t < t^n$; hereafter R^n stands for the interior residual $R^n = I^n f^n - (U^n - I^n U^{n-1})/\tau_n$. The last three terms account for consistency in the constitutive relation, quadrature, and interpolation of the source term; we will refer to them collectively as *consistency terms*. The forth term is similar to the time residual derived in §3, whereas the important new terms are the first three. They will be the focus of our next discussion, and so will be tackled in turn.

In light of (2.4), we readily get

$$\sum_{n=1}^{N} \langle U^{n-1} - I^n U^{n-1}, \phi(\cdot, t^{n-1}) \rangle \le \|\rho\|_{H_0^1(\Omega)} \sum_{n=1}^{N} \|U^{n-1} - I^n U^{n-1}\|_{H^{-1}(\Omega)}.$$

If we integrate by parts at the element level, and rearrange the contributions over each element edge, we obtain

$$-\langle \nabla \Theta^n, \nabla(\phi - \varphi) \rangle = \frac{1}{2} \sum_{S \in \mathcal{M}^n} \langle\!\langle J_S^n, \phi - \varphi \rangle\!\rangle_S,$$

where $\langle\!\langle \cdot, \cdot \rangle\!\rangle_S$ stands for the inner product in $L^2(\partial S)$ and $J_S^n = [\![\nabla \Theta^n \cdot \nu]\!]_S$ is the jump of temperature flux across ∂S, with the convention that the unit normal ν points outwards and $\nabla \Theta^n$ inside S is subtracted from $\nabla \Theta^n$ outside S. We next resort to approximation theory to select φ satisfying

$$\|\phi - \varphi\|_{L^2(S)} + h_S \|\nabla(\phi - \varphi)\|_{L^2(S)} \le C h_S^k \|D^k \phi\|_{L^2(\hat{S})},$$

where $k = 1, 2$ and $\hat{S}$ is the collection of all elements surrounding S; φ could be the Clément interpolant of ϕ. We therefore deduce

$$\begin{aligned} \langle R^n, \phi - \varphi \rangle &\le C_1 \|h_n^k R^n\|_{L^2(\Omega)} \|D^k \phi\|_{L^2(\Omega)}, \\ -\langle \nabla \Theta^n, \nabla(\phi - \varphi) \rangle &\le C_2 |\!|\!| h_n^{k-1/2} J^n |\!|\!|_{L^2(\Omega)} \|D^k \phi\|_{L^2(\Omega)}, \end{aligned}$$

where

$$\begin{aligned} \|h_n^k R^n\|_{L^2(\Omega)}^2 &= \sum_{S \in \mathcal{M}^n} h_S^{2k} \|R^n\|_{L^2(S)}^2 && \textit{interior residual,} \\ |\!|\!| h_n^{k-1/2} J^n |\!|\!|_{L^2(\Omega)}^2 &= \sum_{S \in \mathcal{M}^n} h_S^{2k-1} \|J_S^n\|_{L^2(\partial S)}^2 && \textit{jump residual.} \end{aligned}$$

To continue any further we have to use regularity of the dual solution ϕ. We distinguish two cases, and then compare with the heat equation.

4.1. Approach I. If, according to (2.4), we only assume H_x^1 regularity of ϕ then we see that $k = 1$ and thereby

$$\begin{aligned} \sum_{n=1}^{N} \int_{t^{n-1}}^{t^n} \langle R^n, \phi - \varphi \rangle &\le C_1 \|\rho\|_{H_0^1(\Omega)} \sum_{n=1}^{N} \tau_n \|h_n R^n\|_{L^2(\Omega)}, \\ -\sum_{n=1}^{N} \int_{t^{n-1}}^{t^n} \langle \nabla \Theta^n, \nabla(\phi - \varphi) \rangle &\le C_2 \|\rho\|_{H_0^1(\Omega)} \sum_{n=1}^{N} \tau_n |\!|\!| h_n^{1/2} J^n |\!|\!|_{L^2(\Omega)}. \end{aligned}$$

Collecting all previous estimates we end up with the estimate

$$\frac{|\mathcal{R}(\phi)|}{\|\rho\|_{H_0^1(\Omega)}} \le \sum_{i=1}^{4} \mathcal{E}_i + \text{consistency terms},$$

under minimal regularity of ϕ, where

$$\begin{aligned}
\mathcal{E}_1 &= C_1 \sum_{n=1}^{N} \tau_n \|h_n R^n\|_{L^2(\Omega)} && \textit{interior residual,}\\
\mathcal{E}_2 &= C_2 \sum_{n=1}^{N} \tau_n \|h_n^{1/2} J^n\|_{L^2(\Omega)} && \textit{jump residual,}\\
\mathcal{E}_3 &= \sum_{n=1}^{N} \|U^{n-1} - I^n U^{n-1}\|_{H^{-1}(\Omega)} && \textit{coarsening,}\\
\mathcal{E}_4 &= \Big(\sum_{n=1}^{N} \tau_n \|U^n - I^n U^{n-1}\|^2_{L^2(\Omega)}\Big)^{1/2} && \textit{time residual.}
\end{aligned}$$

Taking now $\delta \downarrow 0$ in (2.6) and using the previous inequality, we deduce the a posteriori error estimate with computable right hand side $\mathcal{E}^{\mathrm{I}}(U, f, T, \Omega; h, \tau)$

$$\|e_u(\cdot, T)\|_{H^{-1}(\Omega)} \le \sum_{i=0}^{4} \mathcal{E}_i + \text{consistency terms} = \mathcal{E}^{\mathrm{I}}. \tag{4.2}$$

4.2. Approach II. If, instead, we assume the degenerate H_x^2 regularity of (2.4), namely $\|D^2\phi\|_{L^2(\Omega)} \le \|\Delta\phi\|_{L^2(\Omega)} \le \delta^{-1/2}\|\rho\|_{H_0^1(\Omega)}$, we get

$$\begin{aligned}
\sum_{n=1}^{N} \int_{t^{n-1}}^{t^n} \langle R^n, \phi - \varphi\rangle &\le \frac{C_1}{\delta^{1/2}} \|\rho\|_{H_0^1(\Omega)} \Big(\sum_{n=1}^{N} \tau_n \|h_n^2 R^n\|^2_{L^2(\Omega)}\Big)^{1/2},\\
-\sum_{n=1}^{N} \int_{t^{n-1}}^{t^n} \langle \nabla\Theta^n, \nabla(\phi - \varphi)\rangle &\le \frac{C_2}{\delta^{1/2}} \|\rho\|_{H_0^1(\Omega)} \Big(\sum_{n=1}^{N} \tau_n \|h_n^{3/2} J^n\|_{L^2(\Omega)}\Big)^{1/2}.
\end{aligned}$$

If we combine these terms with the remaining estimators of Approach I, and insert them back in (2.2), we then readily obtain

$$\|e_u(\cdot, T)\|_{H^{-1}(\Omega)} \le A\delta^{1/2} + B\delta^{-1/2} + \text{remaining terms},$$

where $B = (\mathcal{E}_1^{\mathrm{II}})^2 + (\mathcal{E}_2^{\mathrm{II}})^2$ and

$$\mathcal{E}_1^{\mathrm{II}} = \Big(C_1^2 \sum_{n=1}^{N} \tau_n \|h_n^2 R^n\|^2_{L^2(\Omega)}\Big)^{1/4}, \quad \mathcal{E}_2^{\mathrm{II}} = \Big(C_2^2 \sum_{n=1}^{N} \tau_n \|h_n^{3/2} J^n\|^2_{L^2(\Omega)}\Big)^{1/4}.$$

We can now regard δ as a free parameter and optimize on it, thereby getting $\delta_o = \sqrt{AB}$. Consequently the interior and jump residuals in (4.2) become $\mathcal{E}_1^{\mathrm{II}}$ and $\mathcal{E}_2^{\mathrm{II}}$. Comparing them with $\mathcal{E}_1^{\mathrm{I}}$ and $\mathcal{E}_2^{\mathrm{I}}$, we notice the higher power of meshsize, which may pressumably lead to coarser meshes for the same accuracy, compensated by a smaller outermost exponent; see §6.

4.3. Heat Equation. If we make use of (2.5) and argue as with (3.6), we can write the estimates

$$\sum_{n=1}^{N}\int_{t^{n-1}}^{t^n}\langle R^n,\phi-\varphi\rangle \le C_1\log\frac{T}{\tau_N}\,\|\rho\|_{L^2(\Omega)}\max_{1\le n\le N}\|h_n^2R^n\|_{L^2(\Omega)},$$
$$-\sum_{n=1}^{N}\int_{t^{n-1}}^{t^n}\langle\nabla\Theta^n,\nabla(\phi-\varphi)\rangle \le C_2\log\frac{T}{\tau_N}\,\|\rho\|_{L^2(\Omega)}\max_{1\le n\le N}\|\!|h_n^{3/2}J^n|\!\|_{L^2(\Omega)}.$$

Therefore

$$\frac{|\mathcal{R}(\phi)|}{\|\rho\|_{L^2(\Omega)}}\le C\log\frac{T}{\tau_N}\sum_{i=1}^{4}\mathcal{E}_i^{\mathrm{HE}}+\text{consistency terms},$$

where

$$\begin{aligned}
\mathcal{E}_1^{\mathrm{HE}} &= \max_{1\le n\le N}\|h_n^2R^n\|_{L^2(\Omega)} && \textit{interior residual,}\\
\mathcal{E}_2^{\mathrm{HE}} &= \max_{1\le n\le N}\|\!|h_n^{3/2}J^n|\!\|_{L^2(\Omega)} && \textit{jump residual,}\\
\mathcal{E}_3^{\mathrm{HE}} &= \sum_{n=1}^{N}\|U^{n-1}-I^nU^{n-1}\|_{L^2(\Omega)} && \textit{coarsening,}\\
\mathcal{E}_4^{\mathrm{HE}} &= \max_{1\le n\le N}\|U^n-I^nU^{n-1}\|_{L^2(\Omega)} && \textit{time residual.}
\end{aligned}$$

We realize the powers of meshsize for Approach II correspond to those of the heat operator, but the outermost power as well as the cumulative effect in time are different. In §6 we compare the resulting degrees of freedom for Approaches I and II with those of the heat equation.

5. Adaptive Method. Since the error estimators $\mathcal{E}^{\mathrm{k}}$ of §§4.1, 4.2 entail an L^1 or L^2 accumulation in time, they are impractical in that the entire evolution history would be needed to control the error. The actual a posteriori error estimators thus result from space and time localization at the element level. If $E_h^n(S)$ denotes the contribution to the total error due to an element $S\in\mathcal{M}^n$, then the optimality condition reads

$$E_h^n(S)=\frac{\text{scaled tolerance}}{\text{cardinality of }\mathcal{M}^n}. \tag{5.1}$$

We now explain our strategy for Approach I, just for simplicity, and introduce the element error indicators and all tests necessary for mesh and time step admissibility.

For each $S\in\mathcal{M}^n$, the local spatial error indicators are defined as follows: $E_0(S)$ denotes the initial error and

$$\begin{aligned}
E_h^n(S)=T^2\Big(&C_1^2h_S^2\|R^n\|_{L^2(S)}^2 && \textit{internal residual}\\
&+\tfrac12 C_2^2h_S\|J_S^n\|_{L^2(\partial S)}^2 && \textit{jump residual}\\
&+\tau_n^{-2}\|U^{n-1}-I^nU^{n-1}\|_{L^2(S)}^2\Big) && \textit{coarsening.}
\end{aligned}$$

We also set

$$E_h^n = \Big(\sum_{S\in\mathcal{M}^n} E_h^n(S) \Big)^{1/2}, \quad E_h = \max_{1\le n\le N} E_h^n, \quad E_0 = \Big(\sum_{S\in\mathcal{M}^n} E_0(S) \Big)^{1/2}.$$

We finally define the time residual to be

$$E_\tau^n = T^{1/2}\|U^n - I^n U^{n-1}\|_{L^2(\Omega)}, \quad E_\tau = \max_{1\le n\le N} E_\tau^n.$$

Then it is easy to check that

$$\mathcal{E}^{\mathrm{I}}(u_0, f, T, \Omega; U, h, \tau) \le E_0 + E_\tau + E_h.$$

Let ε be a given *tolerance* for the total error. Given refinement parameters $\Gamma_0 + \Gamma_h + \Gamma_\tau \le 1$ and coarsening parameters $\gamma_h < \Gamma_h$, $\gamma_\tau < \Gamma_\tau$, time steps and mesh densities are reduced until

$$E_h^0 \le \Gamma_0\varepsilon, \quad \gamma_h\varepsilon \le E_h^n \le \Gamma_h\varepsilon, \quad \gamma_\tau\varepsilon \le E_\tau^n \le \Gamma_\tau\varepsilon.$$

This ensures the desired estimate $\mathcal{E}^{\mathrm{I}} \le \varepsilon$. Quasi-optimal meshes are generated by *equidistribution* of the local error estimates $E_h^n(S)$ to all elements of the mesh. The initial mesh is obtained by local refinement of a coarse macro triangulation until $E_h^0(S) \le \Gamma_0^2\varepsilon^2/M^0$ for all $S \in \mathcal{M}^0$, where $M^n = \mathrm{card}\mathcal{M}^n$. In each time step, first the time step size is selected. Starting from τ^{n-1}, the new step size τ^n is reduced until $E_\tau^n \le \Gamma_\tau\varepsilon$. The mesh is adapted so that $\gamma_h^2\varepsilon^2/M^n \le E_h^n(S) \le \Gamma_h^2\varepsilon^2/M^n$ for all elements. This is done by refining all elements S with $E_h^n(S) > \Gamma_h^2\varepsilon^2/M^n$ and by allowing elements with $E_h^n(S) < \gamma_h^2\varepsilon^2/M^n$ to be coarsened. Finally, if $E_\tau^n < \gamma_\tau\varepsilon$, then the initial guess for the next time step size is enlarged. A flow diagram of the adaptive procedure follows:

start with $\mathcal{M}^0$, τ^0, U^0
for $n \ge 1$
  (1) solve for U^n, Θ^n
    compute error estimators E_τ^n and $E_h^n(S)$ for $S \in \mathcal{M}^n$
    if E_τ^n is large, reduce τ^n and goto (1)
  (2) for every $S \in \mathcal{M}^n$
      if $E_h^n(S)$ is large, refine S
      if $E_h^n(S)$ is small, coarsen S if possible
    if the mesh was changed
      solve again for U^n, Θ^n
      compute error estimators
      if E_τ^n is large, reduce τ^n and goto (1)
      if E_h^n is large, goto (2)
    accept U^n, Θ^n and $\mathcal{M}^n$, τ^n
    if E_τ^n is small, enlarge τ^{n+1}

6. Optimal Meshes. We study the relative meshsizes and degrees of freedom for optimal meshes, that is meshes satisfying (5.1). We use the notation h_P and h_H to designate the meshsize away from the discrete interface (parabolic region) and near the interface (hyperbolic region). We also denote with M_P and M_H the corresponding number of elements in these two regions. For simplicity, we only argue with the jump residuals J_S^n and suppress the superscript n. We assume that $M_P = O(h_P^{-d})$, $M_H = O(h_H^{1-d})$ and that $J_S \approx 1$ in the hyperbolic region, $J_S \approx h_P$ in the parabolic counterpart, as expected for a smooth free boundary.
Approach I. Formula (5.1) yields $h_H \|J_S\|^2_{L^2(\partial S)} \approx h_P \|J_S\|^2_{L^2(\partial S)}$, whence

$$h_H \approx h_P^{(d+2)/d}, \quad \frac{M_H}{M_P} = O\big(h_P^{(2-d)/d}\big).$$

We then see that $h_H \approx h_P^2$ for $d=2$, which is consistent with the relation imposed in [10], [11]. Moreover, M_H and M_P are comparable for $d=2$, whereas the former dominates for $d=3$.
Approach II. This time (5.1) implies $h_H^3 \|J_S\|^2_{L^2(\partial S)} \approx h_P^3 \|J_S\|^2_{L^2(\partial S)}$, whence

$$h_H \approx h_P^{(d+4)/(d+2)}, \quad \frac{M_H}{M_P} = O\big(h_P^{(4-d)/(d+2)}\big).$$

We conclude that $M_H \ll M_P$ for $1 \le d \le 3$, and so Approach II requires fewer degrees of freedom than Approach I for a given accuracy. This assertion is confirmed by numerical evidence [12], [14]; see also §8. Since the outermost power of estimators $\mathcal{E}_1^{\mathrm{II}}$ and $\mathcal{E}_2^{\mathrm{II}}$ for Approach II is $1/4$ while it is $1/2$ for the heat equation, we infer that $h_P^{\mathrm{II}} \approx (h_P^{\mathrm{HE}})^2$, and so the heat equation solver requires much fewer degrees of freedom than the best approach for phase change problems.

7. Implementation. This section presents some details about the implementation of local mesh modifications in two and three dimensions and the underlying data structures.

7.1. Mesh Adaptation. We describe the local mesh refinement and coarsening used to adapt the meshes according to information extracted from local error estimators. Several refinement algorithms are available for local refinement of simplicial meshes in two and three space dimensions. Popular methods are *regular refinement* and *bisection*.

With *regular refinement*, triangles are divided into four similar triangles and tetrahedra into eight smaller tetrahedra, with four of these being similar to the original one. Unfortunately, nonconforming nodes arise during local regular refinement, which force additional bisection of some triangles. For tetrahedra, more additional refinement rules are needed for a conforming closure. In order to keep triangulations regular, this additional conforming closure has to be removed before further refinement. This results in (partly) incompatible meshes and introduces interpolation errors between meshes even during refinement operations. The extensions to three dimensions are highly nontrivial, see [2].

In *bisection* methods, instead, elements are divided into two smaller elements by inserting the midpoint of one of their edges, called the *refinement edge*. We use the *newest vertex* bisection, where the refinement edge for a new triangle is chosen as the edge opposite the newly created vertex. For tetrahedra, the choice of refinement edges for new elements is more involved, see [1], [5], [7]; our 3d implementation uses the algorithm described in [5]. Such a choice of refinement edges ensures that shape regularity of the triangulations is preserved, as multiple refinement of single simplices leads to highly regular refined meshes with only few similarity classes of refined elements, as can be seen in Figure 7.1 for the case of refined standard triangle and tetrahedron.

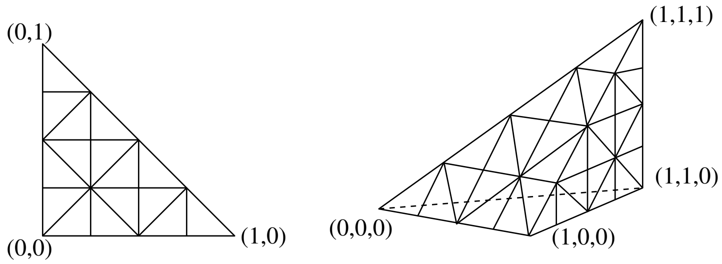

FIG. 7.1. *Refined standard elements in two and three dimensions.*

The refinement algorithm can be implemented using a recursive bisectioning of triangles or tetrahedra. Elements are refined by bisecting their refinement edge. To keep the mesh conforming, bisection of an edge is only allowed when this edge is also the refinement edge for all adjacent elements which share this edge. In 2d there is at most one adjacent triangle, but the number is larger in 3d (6 in Figure 7.3). Bisection of an edge and thus of all elements around the edge is the *atomic refinement operation*, and no other refinement operations are allowed; see Figures 7.2 and 7.3. After each such atomic refinement, the resulting triangulation is conforming. The atomic operation is local in the sense that no elements outside the patch of refined elements are changed.

If an adjacent element to one marked for refinement happens to have a refinement edge other than the common edge, then the adjacent element must be first refined recursively. This generates a compatible refinement edge of the original element and its (new) neighbour. This recursion is guaranteed to stop for every element of a refined triangulation if the recursive refinement does not create cycles on the (usually very coarse) initial triangulation [8]; this can be easily checked for a triangulation with a given choice of refinement edges. For three dimensions, this is proved only under some additional assumptions on the initial triangulation [5]. In Figure

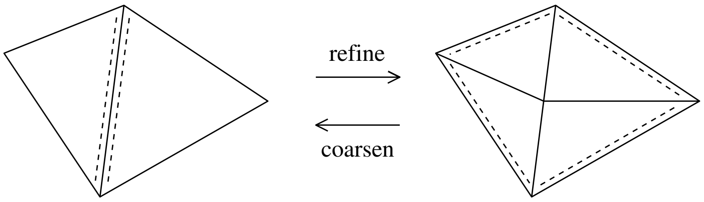

FIG. 7.2. *Atomic refinement and coarsening operations in two dimensions. Refinement edges of triangles are marked with dashed lines.*

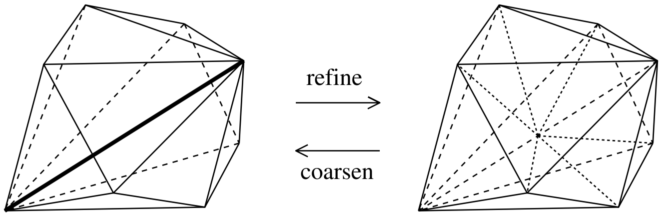

FIG. 7.3. *Atomic refinement and coarsening operations in three dimensions. The common edge is the refinement edge for all tetrahedra around it.*

7.4 we show a situation where recursion is needed. For all triangles, the longest edge is the refinement edge. Let us assume that triangles A and B are marked for refinement. Triangle A can be refined at once, as its refinement edge is a boundary edge. For refinement of triangle B, we have to recursively refine triangles C and D. Again, triangle D can be directly refined, so recursion stops there. This is shown in the second part of the figure. Back in triangle C, this can now be refined together with its neighbour. After this, also triangle B can be refined together with its neighbour.

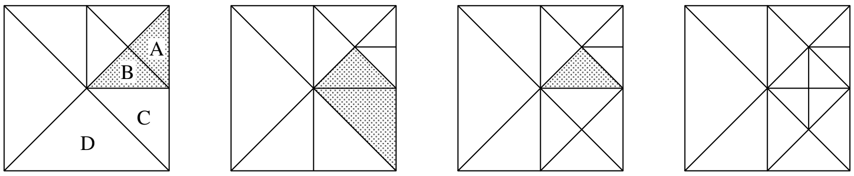

FIG. 7.4. *Recursive refinement. Triangles A and B are initially marked for refinement.*

The inverse operation to atomic refinement is the *atomic coarsening operation*. It reduces a coarsening patch of $2k$ elements into k larger elements. All the smaller elements must have been created together during an atomic refinement operation of the larger ones. Again, the triangulation is still conforming after each atomic coarsening operation and the operation is local in the sense that no elements outside the patch of coarsened elements are changed.

If an element E is marked for coarsening by the adaptive procedure, the basic idea is to collect all those elements which were created together with E by an atomic refinement operation, i.e. the parents of these elements build a compatible refinement patch. If one of these elements is further refined, then coarsening is not possible until such an element is derefined. The entire coarsening patch is coarsened at once provided *all* elements in the patch are marked for coarsening. If one of the elements is not marked for coarsening, we are not allowed to coarsen the patch.

We thus realize the main difference between refinement and coarsening. Every element marked for refinement must be refined even at the expense of additional undesirable refinement. On the other hand, an element marked for coarsening can only be coarsened if all elements of the coarsening patch are also marked for coarsening.

For the usage in the adaptive method described above, elements are marked for refinement if the local estimator $E_h^n(S)$ is larger than the refinement tolerance $\Gamma_h^2\,\varepsilon^2/M^n$, and marked for coarsening if the local estimator is smaller than $\gamma_h^2\,\varepsilon^2/M^n$. In order for the adaptive method to be able to give guaranteed error bounds, the above rules for refinement and coarsening must be enforced.

7.2. Hierarchical Data Structures. The numerical method for Stefan problems in two and three dimensions was implemented with a finite element toolbox written in C, which uses hierarchical data structures for the mesh [15]. Based on the refinement and coarsening by recursive bisection, the refined mesh incorporates naturally the hierarchy of binary trees. The trees are built in such a way that the two smaller elements created by refinement are the two children of the larger parent element. In this way, the whole mesh can be described by a list of binary trees, one for each element of the coarse macro triangulation. Using these data structures, refinement of an element is equivalent to adding two child elements to a tree, while coarsening of elements is equivalent to just removing some leaf elements from the trees. But complete refinement and coarsening patches usually consist of several leaf elements, maybe even from different macro elements, so the atomic operations which are local in mesh geometry are not necessarily local in terms of binary trees.

The hierarchical structure of the mesh makes it possible to generate information like vertex coordinates and element adjacency during tree traversal, thus eliminating the need to store such data for all elements of the mesh. Complete information is stored only for the macro elements. Additional to the sparse mesh storage, the hierarchical data structure provides all necessary information for multilevel methods.

8. Numerical experiments. Our adaptive method is able to detect the presence, and spontaneous appearance, of interfaces and refine accordingly, and is insensitive to topological changes such as merging, extinction, and mush or singularity formation. The interface velocity need not be computed explicitly for mesh design, which is a major improvement with respect to [11]. Further simulations and comparisons with several other nonlinear solvers will be presented elsewhere [14].

8.1. Example 1: Oscillating circle. The exact solution is given by

$$u(x,t) = \begin{cases} \alpha(r^2 - R^2) & \text{if } r \le R \\ 1 + \left(2\alpha R - V \cdot \frac{x-c}{r} - \dot{R}\right)(r - R) & \text{if } r > R, \end{cases}$$

where $r = |x - c|$ and $\alpha > 0$ is a constant, such that $u > 1$ when $r > R$. The interface is thus a circle of center $c(t)$ moving with velocity $V(t) = \dot{c}(t)$ and changing radius $R(t)$. The numerical simulation was done in $\Omega = (-1,1)^2$ for $t \in (0,1)$ with

$$c(t) = (0.25,\, 0.4\,\sin(10\,t)), \quad R(t) = 0.35 + 0.2\,\sin(20\,t), \quad \alpha = 17.0\,.$$

Numerical parameters for the adaptive method were

$$\Gamma_0 = 0.1,\ \Gamma_\tau = 0.2,\ \Gamma_h = 0.6,\ \gamma_\tau = 0.155,\ \gamma_h^{\mathrm{I}} = 0.268,\ \gamma_h^{\mathrm{II}} = 0.190\,.$$

Because of larger meshsize exponents in the estimators, Approach II needs a smaller coarsening parameter γ_h. This prevents alternating coarsening and refinement of elements.

We present results from the two adaptive approaches with tolerances which lead to the same exact errors for temperature and enthaply and thus makes the results comparable. For this reason, the tolerances for Approaches I and II were chosen as $\varepsilon^{\mathrm{I}} = 370$ and $\varepsilon^{\mathrm{II}} = 500$.

Figure 8.1 shows discrete isothermal lines for $\Theta = 0, 2, 4, \ldots$ at different times. The innermost isothermal $\Theta = 0$ is the free boundary. Values (and derivatives) of the solution, along with normal interface velocities, exhibit a large variation in time, depending on R and V. This leads to various levels of mesh refinement and a strong variation in time of the element count, which is shown in Figure 8.2. Both adaptive approaches show a similar behaviour. Approach II, which is represented by the dashed line, leads to fewer elements during several time intervals. This is due to the larger meshsize exponents in the estimators.

Figures 8.3 and 8.4 compare meshes from both adaptive approaches at times corresponding to the isoline pictures. The larger meshsize exponents in estimators from the second approach allow for coarser meshes, while the resolution of the interface is similar in both approaches.

8.2. Example 2: Oscillating source. This is a phase change in a three dimensional container $\Omega = (-1,1)^3$, $T = 20.0$, with initial temperature $\theta(x,0) = 0.1\,(x_1 - 0.2)$, Dirichlet boundary data $\theta(x,t) = \theta(x,0)$, and a spherical heat source oscillating in time,

$$f(x,t) = \cos(0.2\,t)\max\left(0.0,\, 37.0 - 1000\,|x - (-0.5, 0.2, 0.0)|^2\right).$$

The exact solution is not known. Topology of the interface changes during the evolution. Due to the strong heat source, a liquid pool appears inside the solid, which grows and merges with the other liquid part around $t \approx 5.5$. Figure 8.5 displays discrete interfaces at time $t = 0.0, 2.5, 5.0, 7.5$, together with part of the boundary discretization which is clipped in order not to obstruct the interface. Figure 8.6 shows the degrees of freedom over time. Their large variation is mainly due to the strong oscillating source. Figure 8.7 depicts one half of the corresponding tetrahedral meshes with highly refined regions; they capture the interface location along with the presence of the strong heat source.

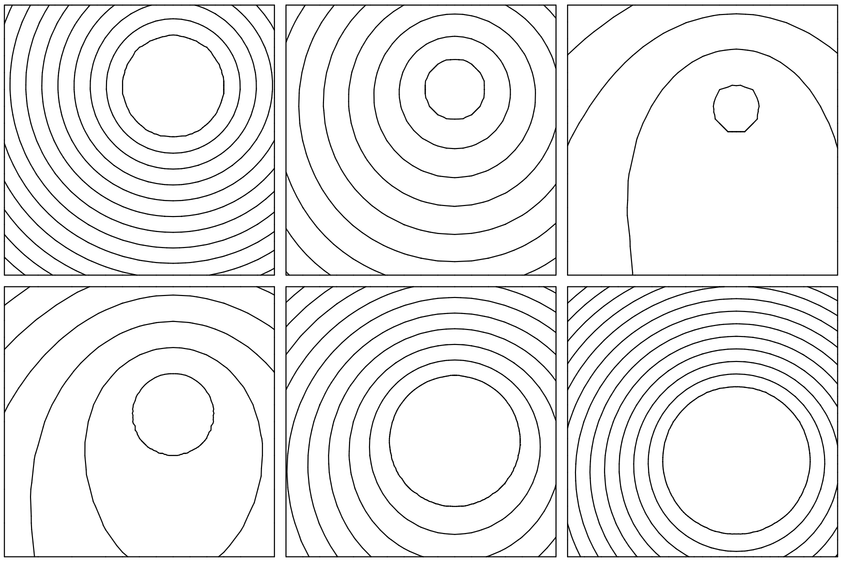

FIG. 8.1. *Example 1: Isothermal lines at* $t \approx 0.15, 0.20, 0.25, 0.30, 0.35, 0.40$.

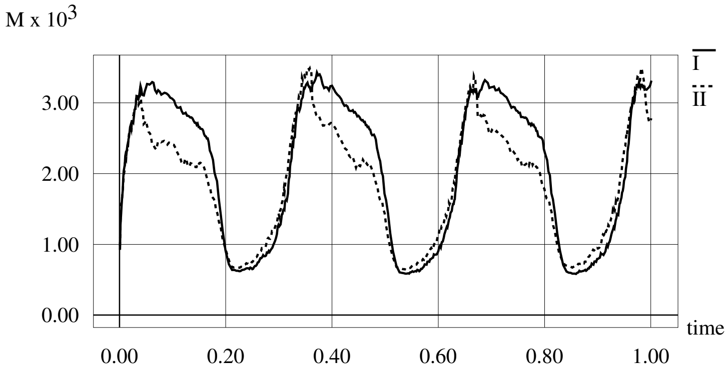

FIG. 8.2. *Example 1: Element counts from Approaches I and II.*

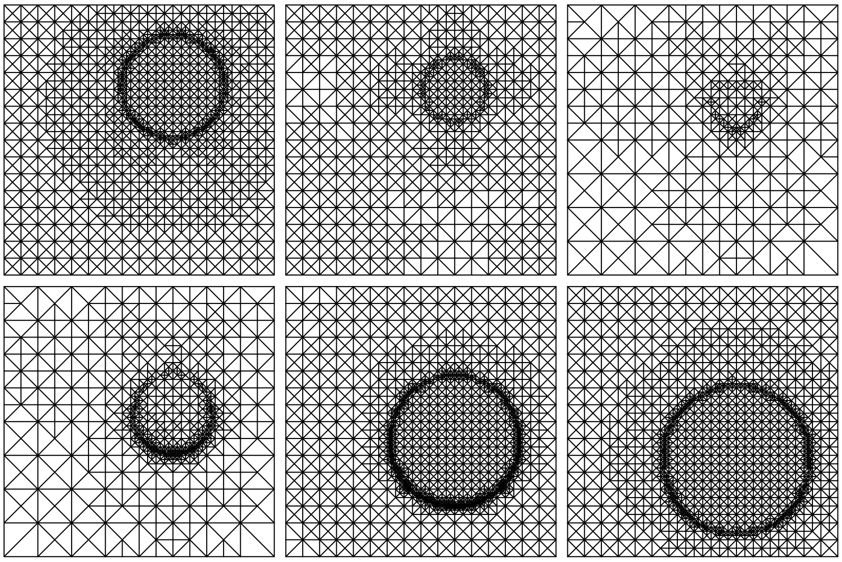

FIG. 8.3. *Example 1: Meshes from Approach I at* $t \approx 0.15, 0.20, 0.25, 0.30, 0.35, 0.40$.

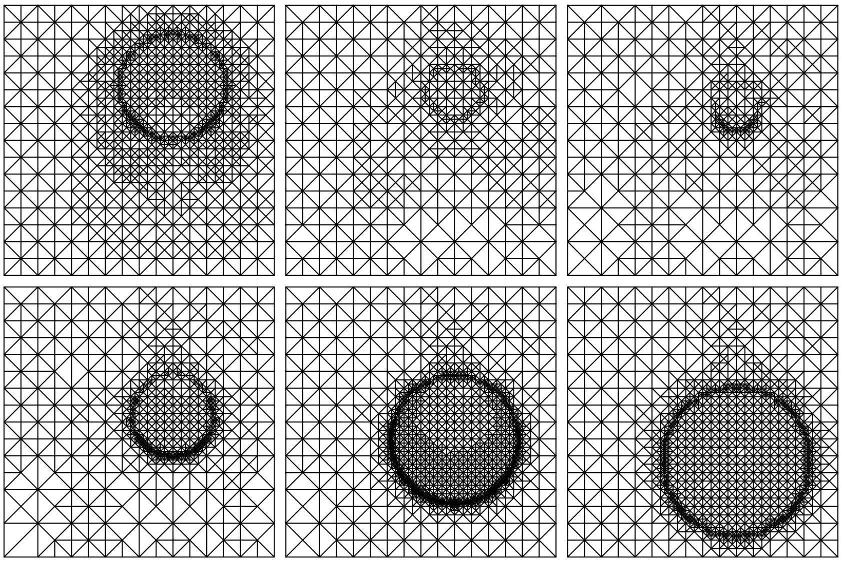

FIG. 8.4. *Example 1: Meshes from Approach II at* $t \approx 0.15, 0.20, 0.25, 0.30, 0.35, 0.40$.

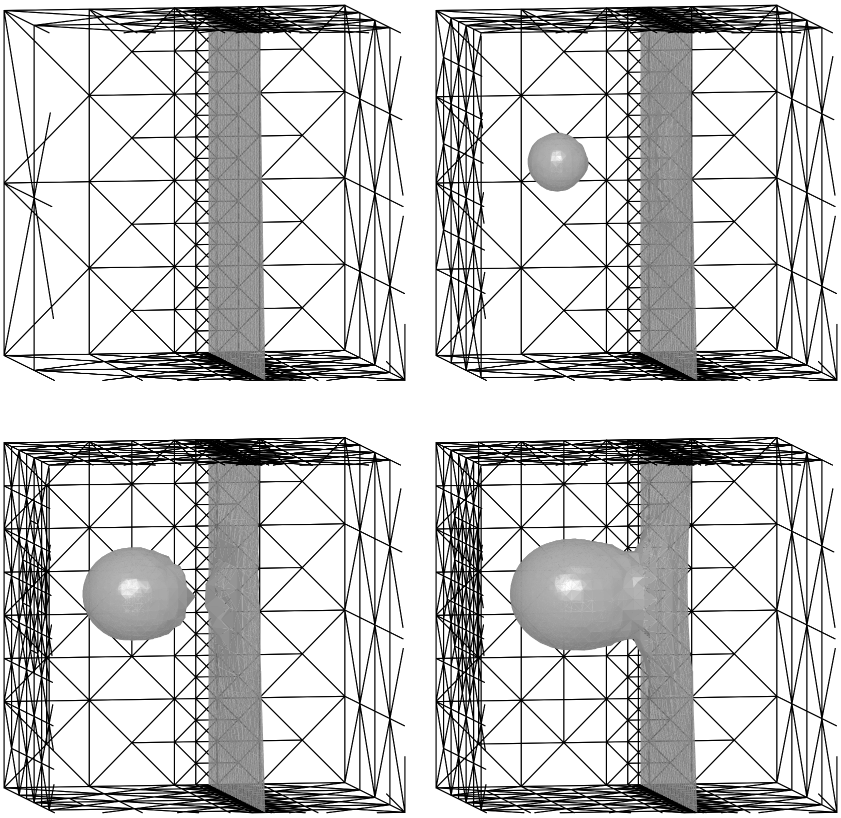

FIG. 8.5. *Example 2: Interfaces at* $t = 0.0, 2.5, 5.0, 7.5$.

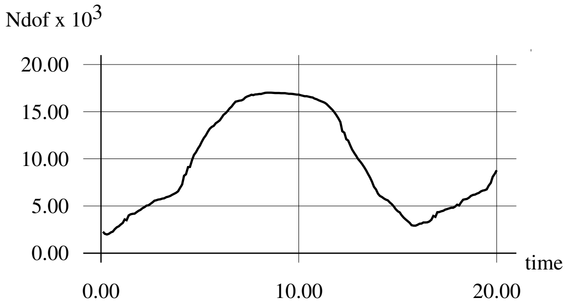

FIG. 8.6. *Example 2: Degrees of freedom over time.*

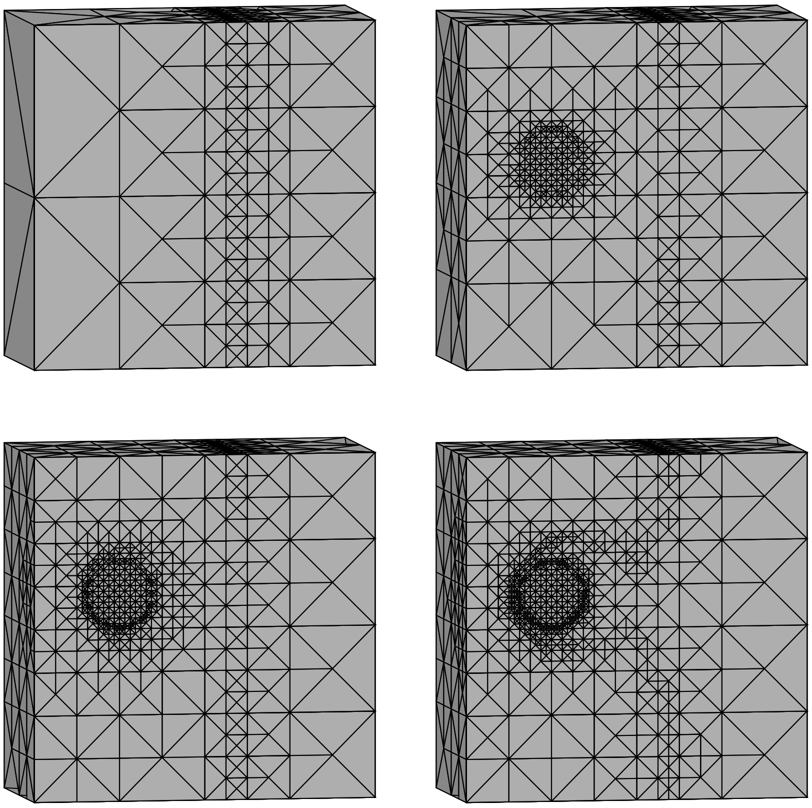

FIG. 8.7. *Example 2: Meshes in* $\Omega \cap \{x_2 \geq 0\}$ *at* $t = 0.0, 2.5, 5.0, 7.5$.

REFERENCES

[1] E. Bänsch, *Local mesh refinement in 2 and 3 dimensions*, IMPACT Comput. Sci. Engrg., 3 (1991), pp. 181–191.

[2] J. Bey, *Tetrehedral grid refinement*, Computing, 55 (1995), pp. 355–378.

[3] K. Eriksson and C. Johnson, *Adaptive finite element methods for parabolic problems I: a linear model problem*, SIAM J. Numer. Anal., 28 (1991), pp. 43–77.

[4] ———, *Adaptive finite element methods for parabolic problems IV: nonlinear problems*, SIAM J. Numer. Anal., 32 (1995), pp. 1729–1749.

[5] I. Kossaczký, *A recursive approach to local mesh refinement in two and three dimensions*, J. Comput. Appl. Math., 55 (1994), pp. 275–288.

[6] O.A. Ladyzenskaja, V. Solonnikov, and N. Ural'ceva, *Linear and Quasilinear Equations of Parabolic Type*, AMS, Providence, 1968.

[7] J.M. Maubach, *Local bisection refinement for n-simplicial grids generated by reflection*, SIAM J. Sci. Comput., 16 (1995), pp. 210–227.

[8] W. Mitchell, *A comparison of adaptive refinement techniques for elliptic problems*, ACM Trans. Math.Softw., 15 (1989), pp. 326–347.

[9] R.H. Nochetto, *Error estimates for multidimensional singular parabolic problems*, Japan J. Indust. Appl. Math., 4 (1987), pp. 111–138.

[10] R. H. Nochetto, M. Paolini, and C. Verdi, *An adaptive finite element method for two-phase Stefan problems in two space dimensions. Part I: Stability and error estimates. Supplement*, Math. Comp., 57 (1991), pp. 73–108, S1–S11.

[11] ———, *An adaptive finite element method for two-phase Stefan problems in two space dimensions. Part II: Implementation and numerical experiments*, SIAM J. Sci. Stat. Comput., 12 (1991), pp. 1207–1244.

[12] R.H. Nochetto, A. Schmidt, and C. Verdi, *A posteriori error estimation and adaptivity for degenerate parabolic problems*, Math. Comp., to appear.

[13] ———, *Mesh and time step modification for degenerate parabolic problems.* In preparation.

[14] ———, *Adaptive algorithm and simulations for Stefan problems in two and three dimensions.* In preparation.

[15] A. Schmidt and K. G. Siebert, *ALBERT: An adaptive hierarchical finite element toolbox.* In preparation.